Dual-band antireflection coatings on 3rd Gen lenses

Thomas D. Rahmlow, Jr.[a], Jeanne E. Lazo-Wasem[a], Jay N. Vizgaitis[b], Justin Flanagan-Hydeb[a]
[a]Rugate Technologies, Inc., 353 Christian Street, Oxford, CT 06478;
[b]US Army RDECOM CERDEC NVESD, Ft. Belvoir, VA 22060

Proc. SPIE 8012, Infrared Technology and Applications XXXVII, 80123D (May 20, 2011)
doi:10.1117/12.888100

Dual-band antireflection coatings on 3rd Gen lenses

Thomas D. Rahmlow, Jr.[a], Jeanne E. Lazo-Wasem[a], Jay N. Vizgaitis[b], Justin Flanagan-Hyde[b]
[a]Rugate Technologies, Inc., 353 Christian Street, Oxford, CT 06478;
[b]US Army RDECOM CERDEC NVESD, Ft. Belvoir, VA 22060

ABSTRACT

Use of a dual band FPA necessitates an optical system that is capable of imaging both mid wave infrared (MWIR) and long wave infrared (LWIR) spectral bands simultaneously. Such optical system can have up to 10 lenses, (20 surfaces that require antireflection (AR) coatings) which, if 95% transmitting in each band, will result in overall throughput of just under 60%[1]. With 99% transmitting in each band, overall throughput would be just over 90%, a relative improvement of 50%. An earlier paper presented dual band antireflection designs, as well as early fabrication attempts on plano Ge, ZnSe, ZnS, AMTIR-1, and CaF_2 windows[2]. This paper presents results of prototype coating fabrication on ZnSe, Ge, and BaF_2 lenses that comprise a 7 lens set. The measured performance of the individual elements is used to model overall system performance. The elements were incorporated into an optical assembly and measured overall imager performance is analyzed and presented.

Keywords: 3rd Gen, infrared, dual band, antireflection, DBAR, mirror, beam splitter, optic

1. INTRODUCTION

Refractive optical designs for high performance dual band infrared imagers using a common focal plane typically call out between 7 and 12 lenses. Three or four different lens materials are typically required to correct for dispersion. The spectral performance for this many surfaces can dramatically impact system throughput. High performance dual band anti-reflection (DBAR) films have been demonstrated[2,3] for a number of commonly used substrate materials including Germanium (Ge), Zinc selenide (ZnSe), Zinc Sulfide (ZnS), and Barium Fluoride (BaF_2). These demonstrations have typically been made on flat substrates. In this paper, we discuss the issues of anti-reflection coating lenses and optimizing performance of the system. Our approaches to coating design, fabrication and metrology are discussed.

The challenge of coating lenses is in obtaining good spectral performance across the optic despite the sag and curvature of the lens. A relatively small difference in height can create a non-uniformity of a few percent across the optic. The curvature of the surface can severely reduce film thickness and performance uniformity still further. Two potential design strategies include either using a broadband design which is relatively insensitive to systematic thickness variation, or more higher performing dual band coatings which are potentially more sensitive. Trade-off studies suggest that, if uniformity on the lens can be held to under 10%, the optimized designs, with appropriate constraints, will outperform broadband designs.

Fabrication requires attention to uniformity control throughout the deposition process. Modeling of source placement and compound rotation allows for uniformity errors across the part to be within 3% for 3 lenses of moderate curvature and, therefore, well within the design uniformity budget.

Characterization of optical transmission of the lenses is also key to enabling the process improvements needed to meet design performance. Establishing good agreement between the optical performance on witness pieces coated in the run, along with the lens and measurements of the lenses, allows for greater confidence in using the witness parts to drive process improvements and modeling of system performance. Techniques for characterizing individual lenses and the lens assembly are being developed.

Different design techniques are needed for low, medium and high refractive index lenses. A seven lens design was selected for coating development and characterization. The 3rd Gen lens set selected for this demonstration (and shown

Infrared Technology and Applications XXXVII, edited by Bjørn F. Andresen, Gabor F. Fulop, Paul R. Norton,
Proc. of SPIE Vol. 8012, 80123D · © 2011 SPIE · CCC code: 0277-786X/11/$18 · doi: 10.1117/12.888100

uncoated in Figure 1 and summarized in Table 1) uses three materials; BaF_2 (low index), ZnSe (medium index), and Ge (high index). All lenses were diamond-turned.

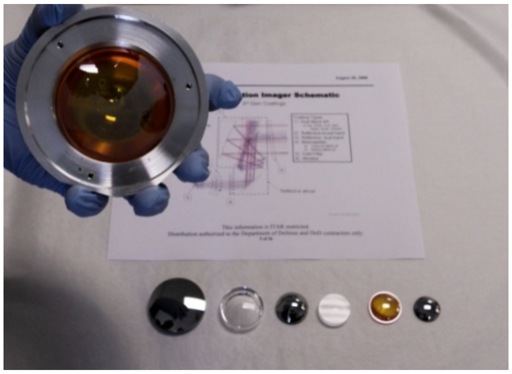

Figure 1: The 7 lens set is shown prior to coating.

Table 1: The 7 lens demonstration set consists of two ZnSe, three Ge, and two BaF_2 lenses

Lens	Material
L1	ZnSe
L2	Ge
L3	BaF_2
L4	Ge
L5	BaF_2
L6	ZnSe
L7	Ge

2. DESIGN

A characteristic of designs which optimize specific spectral regions is that the performance in the target spectral region improves at the expense of performance in the regions that are not of interest. The impact of pushing transmission in the regions of spectral interest typically results in sharp and rapid fall-off of performance in the region just adjacent to the region of interest. The result is that the design can be very sensitive to fabrication errors, non-uniformity of coating thickness such as can occur with a lens due to spectral shift with respect to the local angle of incidence (AOI) on each lens.

Figure 2 presents an overlay of modeled transmission at normal AOI for a broadband AR, one which was optimized only for the spectral region of interest, and for the design with constrained out of band performance at 95, 97 and 98%. The broad band design offers lower performance but relatively little change in performance with systematic changes in the thickness of the film. Figure 3 presents average transmission in the mid-IR region for an assembly of 14 surfaces (7 lenses) for the set of designs presented in Figure 2 as a function of systematically varying the thickness of the film. This systematic variation can occur on a lens as a result of the sag of the surface. In a small chamber with a 20 inch throw height, a 0.25 inch difference in height translates to a 1% variation in film thickness.

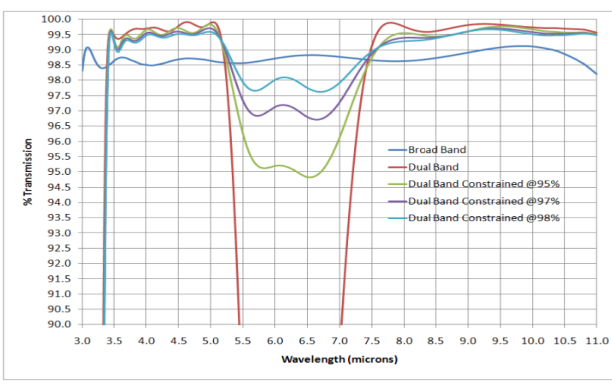

Figure 2: Modeled transmission for a broadband AR, an optimized dual band AR and dual band AR with the out of band region constrained to 95, 97 and 98%. By constraining the out of band region, the impact of thickness errors is reduced.

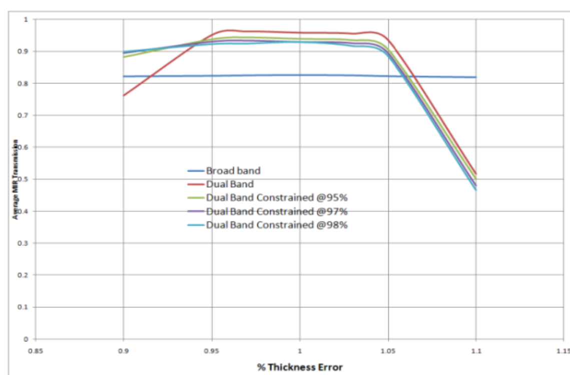

Figure 3: Average MIR Transmission for the 7 lens set of designs in Figure 2 versus % thickness error. Dual band designs have the advantage over broadband when thickness control is better than 6%. The constrained dual designs maintain the advantage out beyond 10% thickness variation.

The dual band AR designs have a performance advantage over the broad band AR design provided errors in deposition on a lens can be held to better than 6%. The dual band constrained AR designs extend this region with tolerable impact on average transmission. In practice, we use a slightly different design for the concave and convex surfaces of a lens. The concave uses a design constrained on the high side of the mid-IR transmission band, and the convex uses a design constrained on the short wavelength side.

The highly optimized design offers high performance, but can be much more sensitive to the local angle of incidence on a lens. An off-axis ray that enters the optical system may experience a wide range of local incidence angles as it passes from lens to lens. If the coating design is too tight or sensitive to angle of incidence, the result can be a significant attenuation of those wavelengths at the longer edge of the passband. The potential design options include making the optimized passband wider, or constraining the out of band regions so that they do not fall off as quickly or as severely as the highly optimized design.

Figure 4 and Figure 5 present the performance of the broad band AR and the optimized dual band AR at 0, 30 and 45^{o} AOI. Interference coatings typically move towards shorter wavelength with increasing angle of incidence. This presents a problem with the optimized dual band design. However, the problem is largely mitigated by constraining the out of band region. A plot of the 97% constrained design for three angles is presented in Figure 6. Figure 7 presents average mid-IR transmission for the set of designs presented in Figure 4.

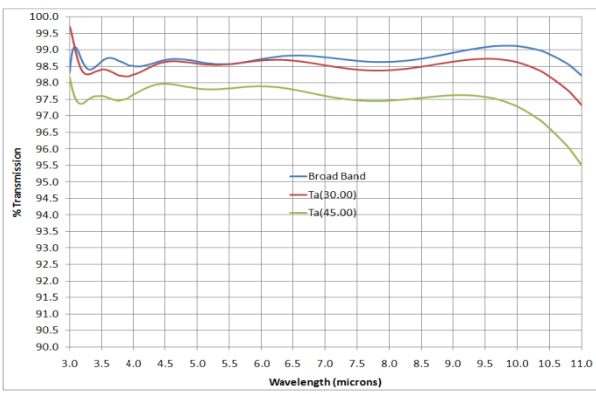

Figure 4: Predicted transmission of the broad band AR design at three angles of incidence (0^{o}, 30^{o}, and 45°).

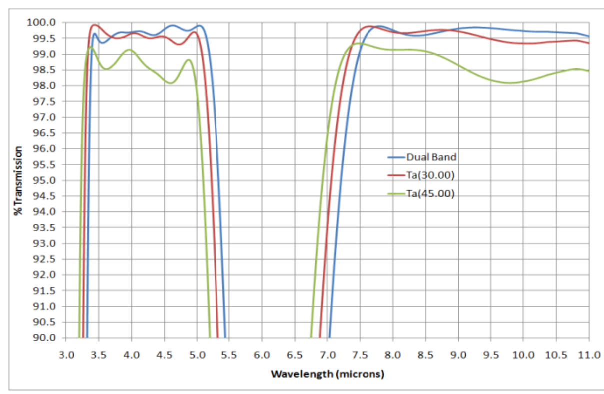

Figure 5: Predicted transmission of the dual band AR at three angles of incidence (0, 30, and 45°).

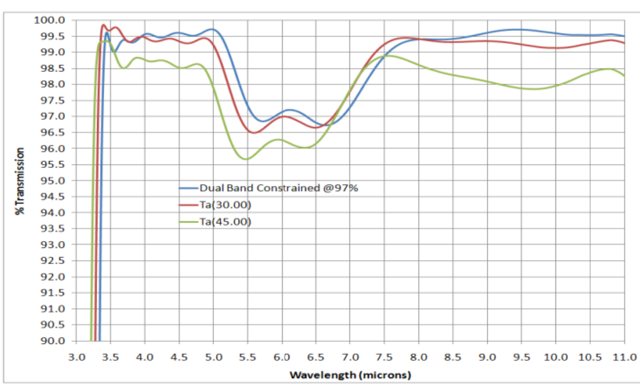

Figure 6: Predicted transmission of the 97% constrained design at three angles (0, 30, and 45° AOI).

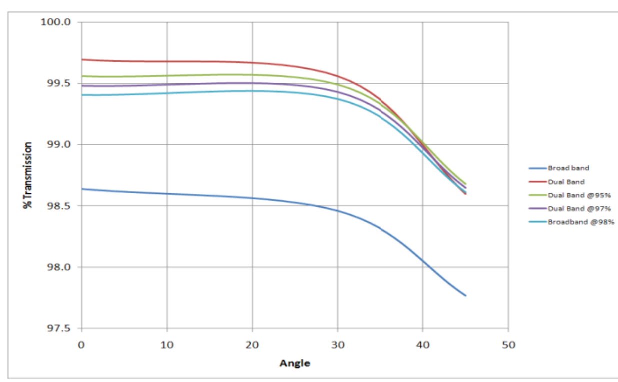

Figure 7: Plot of average mid-IR transmission versus angle for the design set in Figure 4.

The design trade-off between pushing for higher in-band transmission and broadening the design then becomes an issue of optimizing the throughput of the system as it is to be used rather than just optimizing the performance of the coating.
The seven lens system chosen as the baseline system consists of three Ge lenses, two ZnSe lenses, and 2 BaF_2 lenses. The system schematic is presented in Figure 8. Two design sets were selected for coating demonstration. The first set of

designs is optimized for transmission without constraint in the out of band regions. The second set of designs is optimized with constraint at 97% in the region from 5 to 7μm. Figure 9 presents the modeled transmission for each of the lens types. Figure 10 presents predicted transmission for an assembly of seven flats at normal, 30° and 45° AOI, using the first coating design set. Modeled lens transmission and assembly plots are presented in figures 11 and 12 for the dual band design set with constrained out of band transmission.

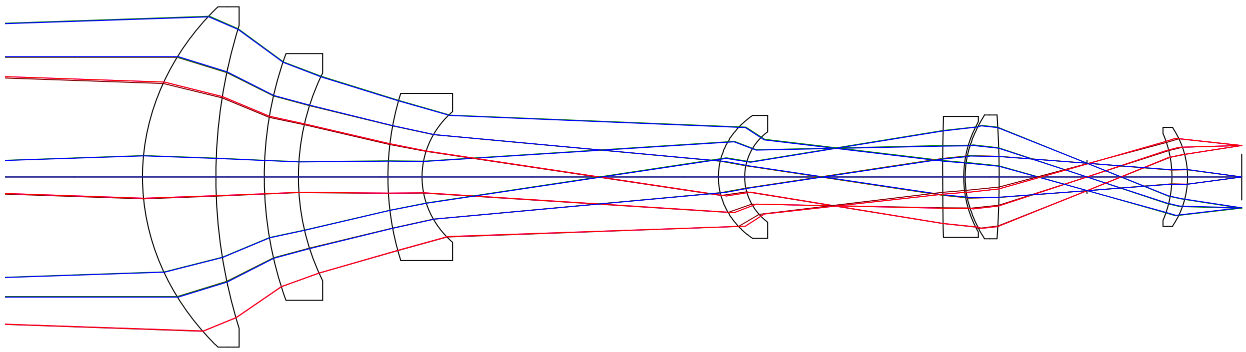

Figure 8: Test lens assembly schematic consisting of seven lenses: 2 ZnSe, 3 Ge and 2 BaF2 lenses.

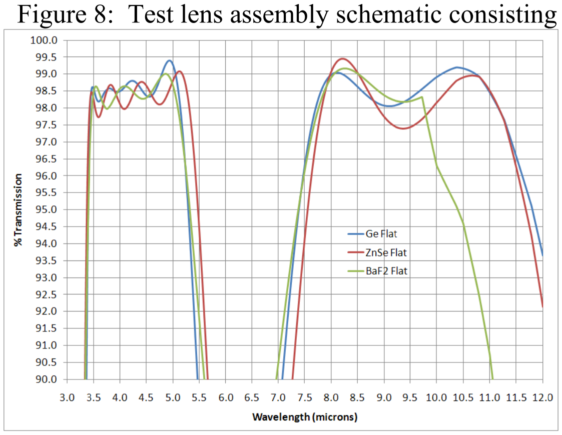

Figure 9: Predicted witness sample transmission for DBAR optimized designs for the three demonstration materials, at normal incidence. The roll off in performance for BaF_2 above 9.5 μm is due to absorption in the substrate.

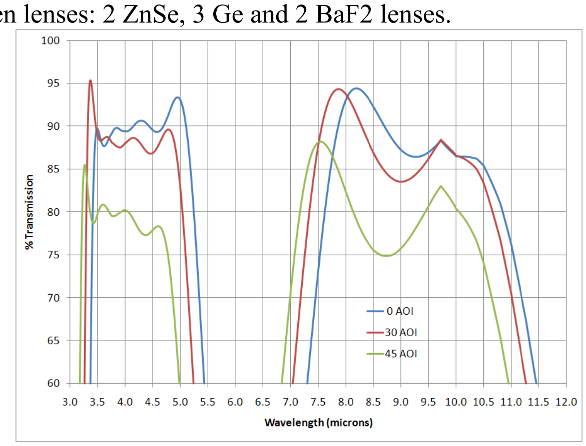

Figure 10: Modeled transmission for an assembly of seven flats at 0, 30 and 45° AOI. The assembly consists of 3 Ge, 2 ZnSe and 2 BaF_2 substrates.

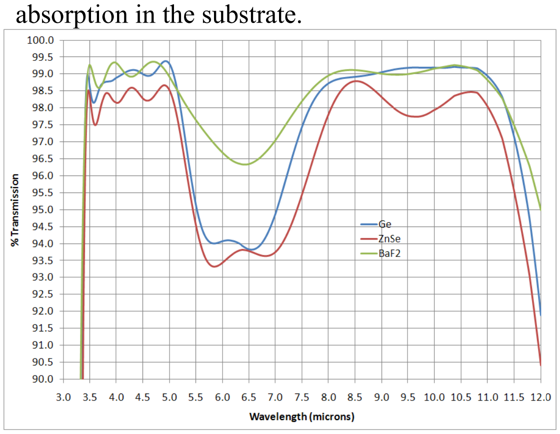

Figure 11: Predicted transmission for DBAR optimized with constrained out of band transmission designs for the three demonstration materials, at normal incidence.

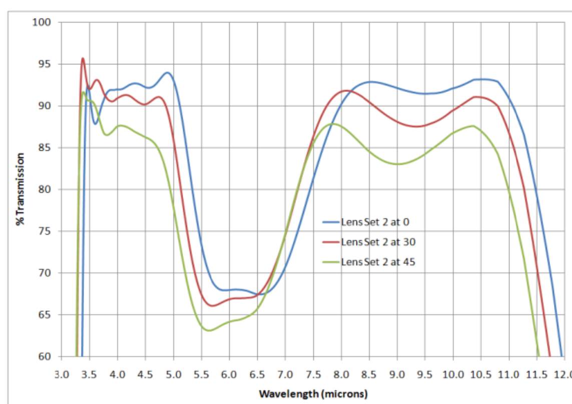

Figure 12: Predicted transmission for the assembly of seven lenses at normal incidence.

The number of layers for the first lens set demonstration designs ranges from 13 to 15 and mechanical thickness from 4.7 to 5.9µm.

Table 2: Design parameters for the lens demonstration

Substrate	Total Thickness	# of Layers	Ave % T 3.5 - 5µm	Ave % T 7.8 – 10.5µm	Ave %T MIR and FIR
Ge	3.66	14	98.4	97.7	98.1
ZnSe	5.86	15	98.9	97.9	98.4
BaF2	4.14	13	98.7	97.6	98.2

3. FABRICATION

Maximizing uniformity for curved substrates is a complex task and involves chamber configuration. Typically, uniformity is optimized experimentally, but since the number of lenses in-hand is limited, the development of a deposition model to explore chamber configuration options is justified. Figure 13 presents a model of thickness uniformity for a curved part moving in compound rotation about the center of the chamber. The position of the sources, crystals and coating plane are presented in the graph on the lower left. The middle graph presents a top down view of the chamber presenting the coating flux for the selected material source at the coating plane, and the path followed by the center of the parts through the coating plane. The graph on the lower right presents a map of the coating flux and of normalized thickness on the part following 100 rotations about the chamber. The graph in the upper right presents a plot of radial thickness across the part and the coating plane (assuming simple rotation). The uniformity for this example varies by 2.72% across 7" part. Our goal is to keep the modeled coating non-uniformity below 3% and thus within the design tolerance.

The coating chamber is Varian 2125 equipped with both resistive sources and a multi-pocket electron beam source. The chamber is evacuated using a CTI Cryo-Torr 10 vacuum pump. The parts are held in tools which enable compound rotation. Deposition temperature was held at 125° C. Coating runs, with time for temperature stabilization, were about 4 hours long.

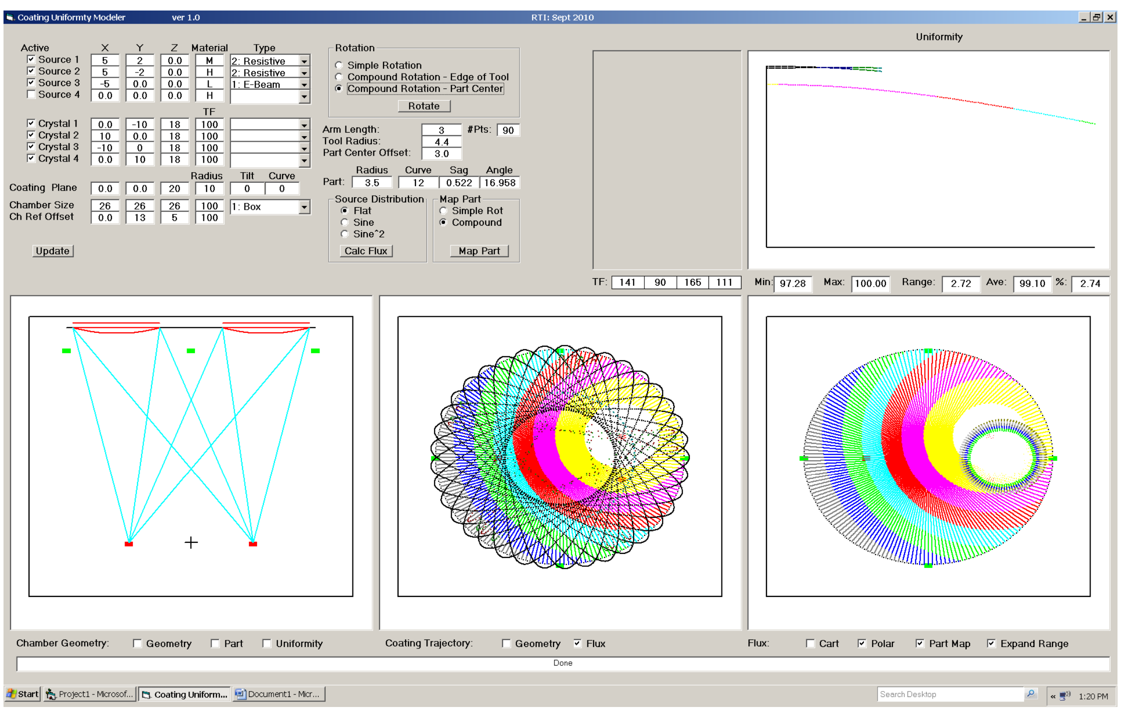

Figure 13: Model of thickness uniformity for a curved part moving in compound rotation about the center of the chamber. The uniformity for this example varies by 2.72% across a 7" part.

4. CHARACTERIZATION

All lenses of the same material were coated in the same lot, along with an equal number of 1" diameter plano witness slides. The selected coatings were deposited on both surfaces. Spectral performance was measured on witness slides from each lot, using a Nicolet 460 Protégé FTIR. Transmission and reflection measurements include substrate absorption, when present. In addition, spectral performance of the lenses was measured individually using an OL-750 monochrometer. Average transmission for MIR and FIR bands using both instruments is shown in Table 4.

The OL-750 double monochromator with IR glower source, followed by a collimator attachment, was used to generate the beam for use in transmission measurements with a HgCdTe detector. Two scans were made for each lens under test (LUT). The calibration scans were made with an empty beam path between the collimator and the detector. The measurement scan consisted of moving the LUT into the beam path. A calibration scan was performed before every measurement scan. Transmission is determined by dividing the measurement scan voltage readings by the calibration scan voltage readings.

Alignment was achieved by a laser directed toward the exit aperture of the collimator attachment with the retroreflection off the LUT used to verify proper alignment. For lenses, an integrating sphere was required immediately before the detector in order to compensate for the irradiance change due to the power of the lens. Use of the integrating sphere results in a 10^{-3} drop in detector signal level. For flats, the integrating sphere is not required.

The exit aperture for the monochromator was a 5mm circular aperture. The exit aperture of the collimator was a 0.5 inch circular aperture so that the effects of beam divergence due to the 5mm aperture, as well as the power of negative lenses, resulted in a beam that was smaller than the entrance aperture of the integrating sphere. The same aperture sizes were used for the flats.

For lenses, both the calibration and the measurement scans used a 2 second dwell time and a 10 second integration time. The calibration scan consisted of three individual scans across the full wavelength range averaged together, and the measurement scan consisted of five individual scans. Measurements were taken with 160nm intervals in the mid-wave IR and with a 320nm interval in the long-wave IR. These intervals are the resolution limit of the monochromator when using the 5mm aperture.

For flats, the much larger signal allows for shorter integration times. The dwell time was 0.5 seconds and the integration time was 0.5 seconds. The calibration and measurement scans still consisted of three and five individual scans respectively and the wavelength intervals were unchanged.

Lenses were measured at normal incidence. Flats were measured at normal incidence individually and as a full set of seven. The full set of flats was also measured with each flat at an angle with respect to the beam axis, once at 15 degrees and once at 30 degrees angle of incidence. The direction of the offset was alternated according to substrate type in order to compensate for beam translation. Measurements for all flats and lenses are shown in Figure 14 through Figure 17.

The measured transmission for the full set of seven flats is 82.55% at normal and is shown at normal and at angle in Table 3. The product of average transmission of the individual flats is 82.74%.

It should be noted that BaF2 begins to absorb about 10µm and, therefore, transmission is limited.

Table 3: Measured average % Transmission across 3.5 - 5µm and 7.8 – 10.5µm (using monochrometer). Direction of angular offset was alternated according to substrate type.

	Average MIR	Average FIR
All 7 flats at 0° AOI	82.78	82.31
All 7 flats at 15° AOI	82.30	82.39
All 7 flats at 30° AOI	79.26	81.51

Table 4: Measured Average % Transmission across 3.5-5 and 7.8-10.5µm for DBAR-coated flat witness samples. The parts were 1mm, 2mm, and 3mm thick for Ge, ZnSe, and BaF2, respectively.

	OL-750	OL-750	FTIR	FTIR
Witness Sample	Average MIR	Average FIR	Average MIR	Average FIR
Flat Ge 11	97.2	98.0	97.5	98.7
Flat Ge 12	97.6	98.1		
Flat Ge 16	97.4	98.4		
Flat ZnSe 15	97.7	96.9	96.8	97.9
Flat ZnSe	97.3	96.3		
Flat BaF_2 3	96.4	96.0	96.3	96.1
Flat BaF_2 4	98.1	97.2		

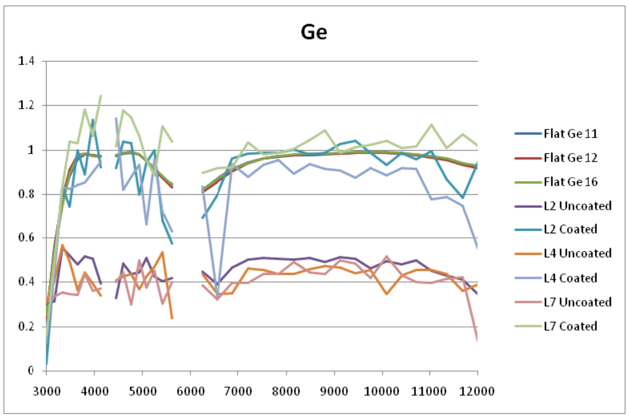

Figure 14: Measured transmission of coated Ge flats and coated and uncoated Ge lenses

Figure 15: Measured transmission of coated ZnSe flats and coated and uncoated ZnSe lenses

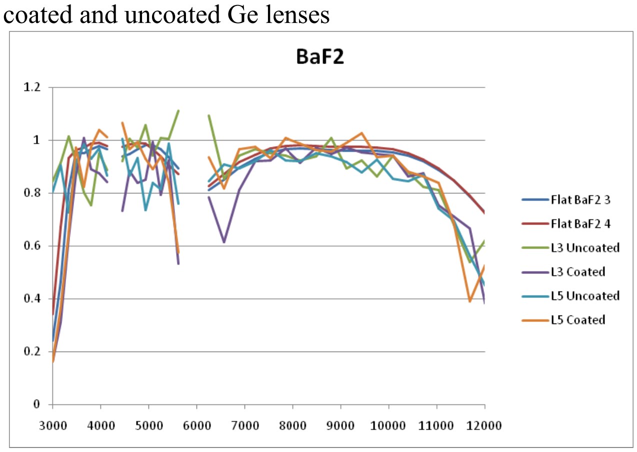

Figure 16: Measured transmission of coated BaF2 flats and coated and uncoated BaF2 lenses

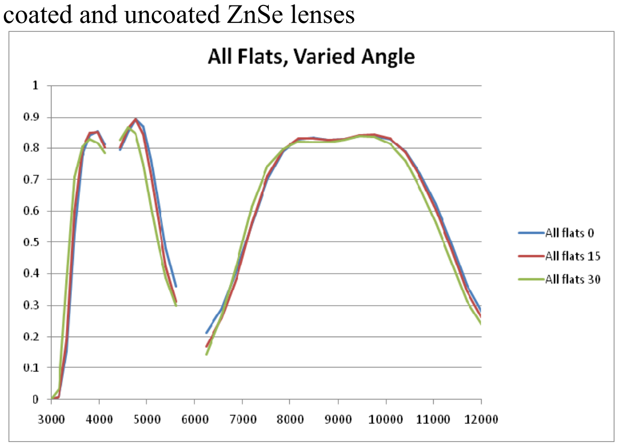

Figure 17: Measured transmission of all coated flats at 0, 15, and 30° AOI

FTIR measurements made on the flat witness pieces, along with predicted performance, are presented in Figure 18 through Figure 20. Measured and predicted performance of the assembly at normal AOI are presented in Figure 21. The photographs in Figure 22 and Figure 23 illustrate the assembly measurement technique.

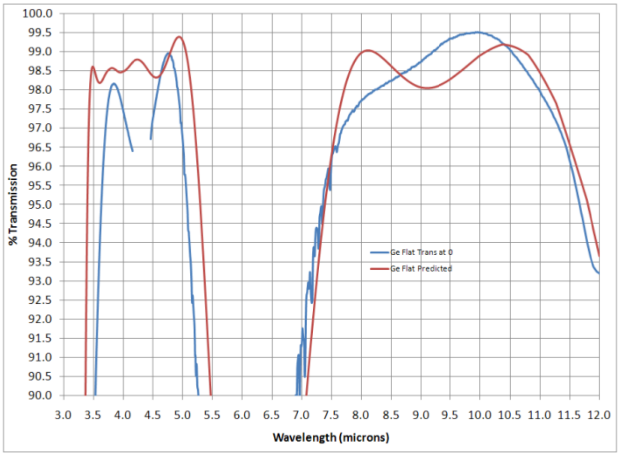

Figure 18: Predicted performance and FTIR measurements for the Ge witness flats from the first lens set.

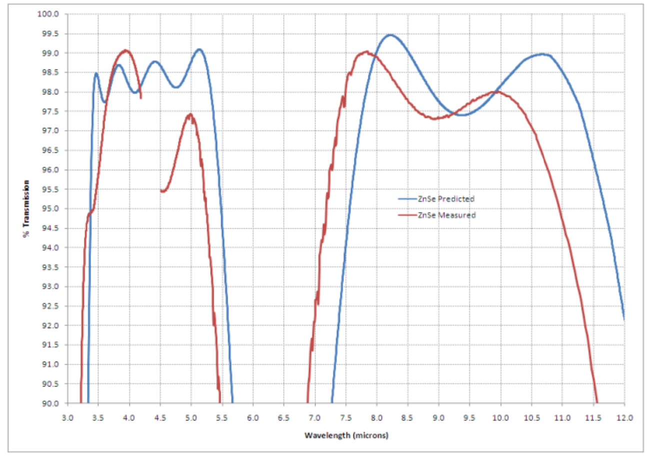

Figure 19: Predicted performance and FTIR measurements for the ZnSe witness flats from the first lens set.

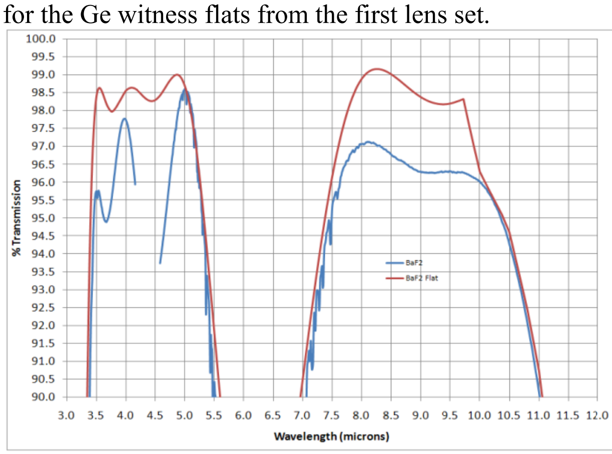

Figure 20: Predicted performance and FTIR measurements for the BaF_2 witness flats from the first lens set.

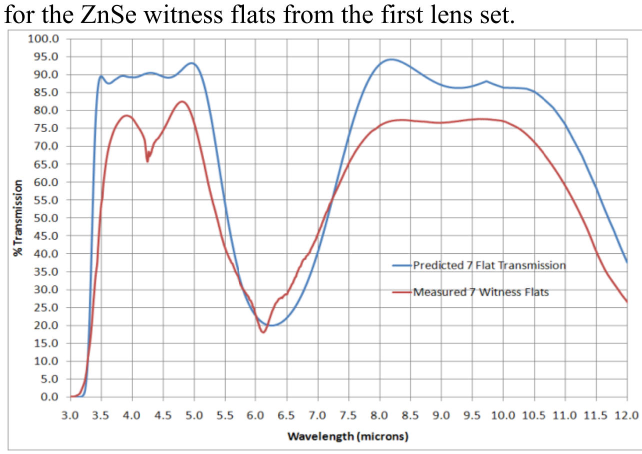

Figure 21: Predicted performance and FTIR measurements for the assembly of 7 witness parts at normal AOI.

Figure 22: Transmission of witness sample assembly measured at normal incidence

Figure 23: Transmission of witness sample assembly measured at 30° AOI

5. CONCLUSIONS

The design trade-off between broad band and dual band designs was compared. It is found that the dual band designs, while more sensitive to systematic thickness variation than broad band designs, offer better spectral performance as long as the systematic errors in film thickness can be limited to 6% or so. The highly optimized dual band designs can be desensitized by confining out of band regions with only minimal impact on average spectral performance.

Desensitizing the design to variations in film thickness reduces the need to use lens-specific masking during the coating process, provided coating uniformity can be achieved using compound rotation.

This effort was the first demonstration of designing, coating, and characterizing DBAR films on a 3rd Gen set of lenses. Comparisons between predicted and measured performance were established and provide a baseline of performance. Additional lens sets will be coated and performance will be compared to these results in ongoing process improvement efforts.

A method of characterizing optical performance on lenses was established. Good agreement between optical measurements on flat witness pieces and lenses was demonstrated. This supports the claim that the desensitization of the design and chamber tooling was adequate. This also allows for greater confidence in using witness parts to drive process improvements.

REFERENCES

[1] Vizgaitis, J., “Third Generation Infrared Optics”, Proc. SPIE 6940-26 (2008).

[2] Rahmlow, T.D., Jr., “Dual-band antireflection coatings for the infrared”, SPIE 6940-26 (2008).

[3] Rahmlow, T.D., Jr., “Filters for dual band infrared imagers”, SPIE 7298-87 (2009).

[4] Vizgaitis, J., et. al., “3rd Demonstration FLIR Demonstrator”, SPIE 6940-OU (2008).

[5] Snyder, Miguel, and Vizgaitis, J., “Optical design study for the 1 – 5micron spectral band”, SPIE 7298-10 (2009).

[6] Tamagama, Y., and Tajime, T., “Dual-band optical systems with a projective athermal chart: design”, Applied Optics, Vol. 36, No. 1, pp 297-301 (1997).

[7] Goldberg, A., et. al., “Dual-Band Imaging of Military Targets Using a QWIP Focal Plane Array”, DTIC (2001).